Template-controlled acidity and catalytic activity of ferrierite crystals

A.B. Pinar, C. Márquez-Álvarez, M. Grande-Casas, J. Pérez-Pariente *

Instituto de Catálisis y Petroleoquímica (CSIC), c/ Marie Curie 2, Cantoblanco, 28049-Madrid, Spain

ARTICLE INFO

ABSTRACT

A synthesis strategy to tailor the acid sites location in ferrierite crystals has been developed. The zeolite catalysts were synthesised in fluoride medium using different combinations of organic structure directing agents (SDAs) in the absence of inorganic cations. Therefore, the negative charge associated to the incorporation of aluminium to the framework was compensated exclusively by the positive charge of the organic SDAs. In this way, Al sitting in the zeolite framework was driven by the specific location of the different SDA molecules within the zeolite void volume. Following this synthesis strategy, it has been found that the distribution of strongly acidic hydroxyl groups in the proton form of the zeolites obtained after removal of the organic templates was dependent on the combination of organic molecules used as SDAs. Moreover, the catalytic activity of the zeolites in *m*-xylene and 1-butene isomerisation increased as the relative population of strong Brönsted acid groups in sterically constrained sites inside the ferrierite cavity decreased.

1. Introduction

Activity and selectivity patterns of a particular acid zeolite in different catalytic reactions are recognised to depend upon the combination of several factors, the number and distribution of acid sites in the framework among them. Controlling the distribution of framework aluminium atoms, and hence that of the acid sites, in zeolites is a much sought objective in zeolite research, as it would have a strong impact on catalytic activity and selectivity. Indeed, it has been shown for ZSM-5 [1–3] and MCM-22 [4] that Al distribution is dependent on the Si/Al ratio and on the synthesis procedure.

The presence of different types of cavities for a given zeolite topology introduces a high degree of complexity in the distribution of acid sites. Many interesting zeolite catalysts possess precisely the complex void architecture that makes them suitable candidates for the development of specific synthesis strategies envisaging to control the aluminium sitting and hence the acidity of the structure. Ferrierite is one of such materials. Its structure consists of channels of 10-membered rings (10-MR, a ring constituted by 10 T atoms linked through T–O–T bonds, where "T" represents a Si or an Al atom tetrahedrally coordinated to 4 oxygen atoms) running parallel to the crystallographic [001] direction, which are intersected by 8-MR channels parallel to the [010] direction. In addition, 6-MR

channels run along the [001] direction. The intersection of these 6-MR channels with the above mentioned 8-MR channels leads to the formation of the "ferrierite cavity", a $[8^2 6^2 6^4 5^8]$ cage accessible through 8-MR windows [5]. The ferrierite framework was first determined in the space group *Immm* [6] although reductions of symmetry have been reported [7–9]. In Fig. 1 a representation of the structure can be seen, showing the 4 non-equivalent T atoms (in space group *Immm*) and their accessibility from the 10-MR channel and the cage. It has been shown before [10–12] that this zeolite can be conveniently synthesised in the absence of alkaline cations by using an appropriate combination of small and large structure directing agents (SDA). In particular, the hydrothermal treatment of synthesis gels containing both 1-benzyl-1-methylpyrrolidinium (bmp) and tetramethylammonium (TMA) cations in fluoride medium allows the crystallisation of zeolite ferrierite. Furthermore, computational studies reveal that TMA cations are located inside the small cages, while the large and elongated bmp cations are placed in the 10-MR straight channel. Hence, both cations cooperate to build up the ferrierite structure. Moreover, in the absence of either bmp or TMA, ferrierite was not obtained, thus showing the key role of both cations in the crystallisation of this zeolite in these synthesis conditions. As far as no alkaline cations are present in the structure, the charge compensation of the aluminium atoms located in the framework is due to the cationic SDA only. Using CP-MAS NMR and heteronuclear correlation NMR, Lobo et al. [13] found that the positively charged fragment of the SDA is preferentially ordered near the negative frame-

* Corresponding author. Fax: +34 91 5854760.
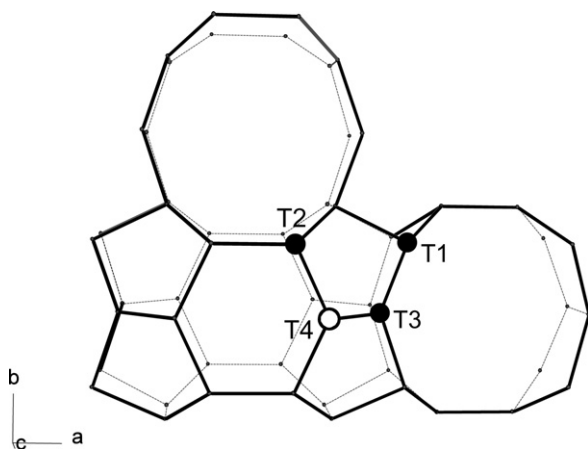*E-mail address:* jperez@icp.csic.es (J. Pérez-Pariente).

Fig. 1. Framework structure of FER showing the 4 non-equivalent T-atoms (in space group *Immm*). T1, T2 and T3 (black atoms) are accessible from the 10-MR channel and from the FER cavity. T4 (white atom) is accessible only from the cavity. Bridging oxygen atoms have been omitted for clarity.

work charge in ZSM-12, and suggested that the location of acid sites in the zeolite might be controlled by the charge distribution of the SDA. It could be then conceived that the framework sites occupied by aluminium in ferrierite would be eventually dependent upon the specific combination of SDAs used in the synthesis. Moreover, it has been evidenced that the extra-framework charge-compensating cation distribution in ferrierite zeolites changes as a function of their Si/Al ratio [14], and from this feature it has been concluded that the Al distribution among the different T sites is affected as well.

Based upon these previous studies, we report in this work a new approach aiming to influence the aluminium location in ferrierite. Our hypothesis is that the use of a combination of organic molecules as SDAs can influence the distribution of acid sites of the zeolite obtained, i.e., the particular combination of SDAs employed in each case could have an effect on the population of aluminium in the different T sites of the zeolite. Therefore, our synthesis strategy consists on the use of a combination of different organic molecules acting as co-structure directing agents, in the absence of sodium cations. This is an important aspect, as the negative charge associated to the incorporation of aluminium to the tetrahedral sites by isomorphic substitution of silicon will be compensated exclusively by the positive charge of the organic SDAs. Following the previous synthesis approach using bmp and TMA as SDAs, ferrierite samples have been obtained from gels in which the bulky bmp cation has been substituted by pyrrolidine (pyrr) and then both bmp and TMA have been replaced by pyrrolidine, i.e., only pyrrolidine has been used as SDA, always maintaining a constant total concentration of organic compounds. For comparison purposes, a ferrierite sample has been prepared by using pyrrolidine at high pH in presence of sodium cations [15]. The acidity of the calcined materials has been investigated by FTIR spectroscopy and pyridine adsorption, and their catalytic activity in *m*-xylene and 1-butene isomerisation has also been determined.

2. Experimental and methods

2.1. Synthesis of the SDAs

The synthesis of bmp was carried out by methylation of benzylpyrrolidine as reported earlier [10]. The purity of the tertiary amine was assessed by thin layer chromatography (hexane/ethyl acetate as solvent) and chemical analysis (calculated values, in wt%: C 82.0; N 8.7; H 9.3; found: C 81.5; N 8.7; H 9.9).

Benzylpyrrolidine was methylated with methyl iodide (50% molar excess, Fluka) in ethanol. The stirring was maintained for 5 days at room temperature and ethanol was then removed under vacuum at 60 °C. The resulting solid benzylmethylpyrrolidinium iodide was exhaustively washed with diethyl ether until the resulting liquid was colourless. The composition of the collected yellow solid was determined by chemical analysis (calculated values, in wt%: C 47.5; N 4.6; H 5.9; found: C 47.3; N 4.7; H 5.8), while ^{13}C CP MAS-NMR confirmed the integrity of the benzylmethylpyrrolidinium cation (bmp). The iodide salt was then converted into the corresponding hydroxide salt (bmpOH) by ion exchange through an Amberlyst IRN78 resin (exch. cap.: 4 meq/g, Supelco). The obtained solution of bmpOH was filtered to remove the resin and titrated with 0.05 M HCl (Panreac) using phenolphthalein (Aldrich) as an indicator.

2.2. Synthesis of the zeolites

Zeolite products synthesised in fluoride medium were obtained following the synthesis procedure reported earlier [10] from synthesis gels in which the molar ratio organic/T atoms was kept constant. The molar gel composition for the samples with bmp and TMA as SDAs was: 0.969 SiO_2:0.031 Al_2O_3:0.06 TMAOH:0.48 bmpOH:0.48 HF:4.6 H_2O. For the samples prepared with TMA and pyrrolidine as SDAs, the same gel composition was employed, substituting bmp by pyrrolidine. For the samples prepared in the presence of pyrrolidine as the only SDA the same molar composition was used but with molar ratio pyrr:(Si + Al) = 0.54, thus maintaining the ratio organic compounds/T atoms constant. The Si/Al ratio in the gel was 15.7 in all the cases. In the synthesis gels in which TMA is one of the SDAs, the ratio TMA/Al was 1.
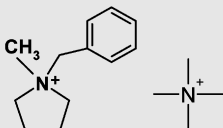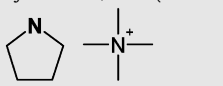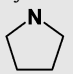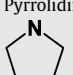
All these samples underwent a post-synthesis treatment in order to get their catalytically active form. They were heated in nitrogen flow up to 200 °C and kept at this temperature for 2 h, followed by a treatment with a flow of oxygen enriched in ozone (60 mL/min, ca. 2 vol% ozone) at 200 °C to remove, in mild conditions, the organic molecules employed as SDAs. An ECO-5 ozone generator (Salveco Proyectos, S.L.) was employed to produce the ozone-enriched oxygen stream. In the final step prior to their use as catalysts the samples were heated in an air flow for 2 h up to 550 °C and kept at this temperature for 2 additional hours.

The sample synthesised in alkaline medium following the conventional procedure, FER1, crystallised from a gel with the following molar composition: 0.969 SiO_2:0.031 Al_2O_3:0.323 pyrrolidine:0.049 Na_2O:11.95 H_2O. The gel was heated at 175 °C and autogeneous pressure for selected periods of time, and then it was filtrated, washed and dried overnight. The same treatment in an ozone-enriched stream was applied to remove the organic material occluded within the zeolite. The calcined product was subsequently ion-exchanged with a 1 M ammonium chloride solution (Probus, 99.5 wt%) to eliminate Na^+ cations, which were substituted by ammonium cations in this process. For this purpose the zeolite was placed in a round-bottomed flask with the ammonium chloride solution (1 g zeolite/100 mL solution) and it was stirred at 80 °C for 8 h under reflux. Then the solid was recovered by filtration and washed exhaustively with deionised water to eliminate chloride and sodium ions. This procedure was repeated twice, maintaining the stirring for 12 and 24 h, respectively. Complete removal of chlorine ions was confirmed by the absence of AgCl (white solid precipitated) when adding silver acetate solution to the filtrate. The sample was dried overnight and calcined in an air atmosphere for 3 h at 350 °C and 3 h at 550 °C to decompose ammonium ions, thus obtaining the zeolite in its proton form.

Hereafter, the ferrierite samples will be denoted making reference to the organic cations employed as SDAs in their synthesis, separated by a dash if two different molecules are em-

Table 1
Summary of the syntheses carried out with the different combinations of SDAs. The heating temperature was 175 °C for FER1 samples and 150 °C for the rest of the samples.

| Sample	SDA	t (days)	pH gel
	TMA + bmp (fluoride medium)		
FER-bmp-TMA		10 20 30 83	10.2
	Pyrrolidine + TMA (fluoride medium)		
FER-pyrr-TMA		7 10	8.6
	Pyrrolidine (fluoride medium)		
FER-pyrr		7 10	7.4
	Pyrrolidine (alkaline medium)		
FER1		14	12.1

Fig. 2. XRD patterns of samples FER-pyrr (a), FER-pyrr-TMA (b) both obtained after 10 days of hydrothermal treatment, FER1 (c) obtained after 14 days and FER-bmp-TMA (d) obtained after 20 days. The peak highlighted with an asterisk corresponds to an unidentified dense phase. In all cases the pattern corresponds to the calcined sample.

ployed together as a combination of SDAs: FER-bmp-TMA (synthesised with 1-benzyl-1-methylpyrrolidinium and TMA), FER-pyrr-TMA (with pyrrolidine and TMA), FER-pyrr (with pyrrolidine) and FER1 (with pyrrolidine in aqueous alkaline medium in the presence of sodium). Table 1 summarises the syntheses carried out with the different combinations of SDAs.

2.3. Characterisation of the solids

Solid products were characterised by XRD (PANalytical X´Pert PRO-MPD diffractometer, CuKα radiation), thermal analysis (Perkin–Elmer TGA7 instrument, heating rate 20 °C/min, air flow 30 mL/min, temperature range 20–900 °C), chemical CHN analysis (Perkin–Elmer 2400 CHN analyser), ICP-AES (Optima 3300 DV Perkin–Elmer) and SEM/EDX (Jeol JSM 6400 Philips XL30, operating at 20 kV). ^{27}Al MAS NMR spectra were recorded with a Bruker AV 400 spectrometer using a BL4 probe. Pulses of 1 μs were used to flip the magnetisation, with $\pi/12$ rad, and delays of 1 s between two consecutive pulses. The spectra were recorded while spinning the samples at ca. 11 kHz.

Transmission FTIR spectra were recorded in the 400–4000 cm^{-1} range, at 4 cm^{-1} resolution, using a Nicolet 5ZDX FTIR spectrometer provided with an MCT detector. The samples were pressed into self-supporting wafers (ca. 6 mg/cm^2 thickness), placed in a glass cell with CaF$_2$ windows, and activated in vacuum at 400 °C for 8 h. Pyridine adsorption was carried out on activated samples kept at 150 °C, and followed in dependence of time. The sample wafer was put in contact with pyridine vapour (8 Torr) at 150 °C for a given period of time, subsequently degassed at the same temperature for 30 min, and then the FTIR spectrum was recorded. Pyridine was again dosed into the cell to allow further adsorption of pyridine on the wafer, and the cell was evacuated for 30 min prior to recording the FTIR spectrum. This adsorption procedure was repeated several times in order to obtain a series of FTIR spectra at increasing total contact time of the sample wafer with pyridine. The spectra recorded after pre-treatment and after every pyridine adsorption step were normalised to a sample thickness of 6 mg/cm^2.

2.4. Catalytic activity

The catalytic activity of the samples was tested in the isomerisation of m-xylene reaction; m-xylene was purchased from
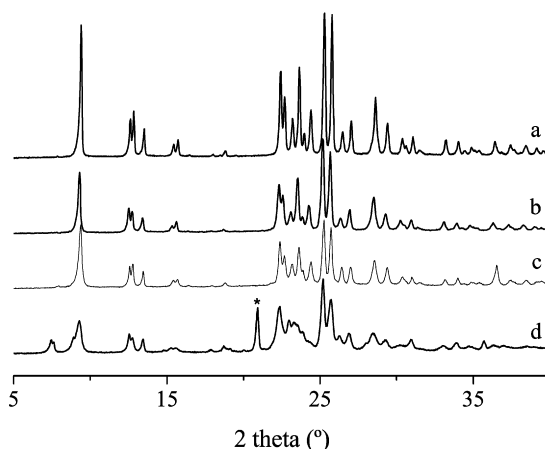
Scharlau (99%). These experiments were carried out in a differential fixed-bed reactor operating with continuous feed and nitrogen as carrier gas at atmospheric pressure. All the samples were previously activated in air flow (100 ml/min) at 450 °C for 1 h. Then the flow was changed to N$_2$ and the temperature decreased to 350 °C, keeping these conditions for 1 more hour, after which the reaction is performed at the same temperature. In order to obtain conversions of about 5%, the contact time was varied, while the molar ratio was fixed at N$_2$/m-xylene = 5.3. The reaction products were analysed by gas chromatography using a 2 m × 3 mm OD packed column filled with 16% DC-200 methylsilicone and 3% Bentone 34 on 80–100 mesh ChromosorbW. A Varian 3800 gas chromatograph provided with a flame ionisation detector (FID) was used in the analysis. In order to compare the activity of the catalyst in the absence of deactivation, the initial activity (V_0) of all products were calculated by extrapolating the conversion at time zero of reaction.

The transformation of 1-butene was carried out in an automatic fixed-bed reactor under the following conditions: 400 °C, atmospheric pressure, N$_2$/butene molar ratio 4, weight hourly space velocity (WHSV) of 25 h^{-1}. The catalysts samples ≈100 mg (pelletised and sieved to 0.84–0.42 mm) were previously pre-treated in situ under nitrogen flow for 1 hour at 400 °C. The products were analysed on-line by gas chromatography using a capillary column (PLOT Al$_2$O$_3$ 50 m × 530 μm). A Varian Cp-3880 gas chromatograph provided with a flame ionisation detector (F.I.D.) was used in the analysis. The conversion into the different products was calculated by considering n-butene isomers as the reactant. The activity at 30 min time-on-stream was used to compare catalytic performance.

3. Results and discussion

3.1. Synthesis of the materials

Pure zeolite ferrierite crystallised from the three different synthesis gels prepared in fluoride medium. Fig. 2 collects the XRD patterns of the corresponding products. It can be observed that the solids obtained in the absence of bmp present sharper diffraction peaks, which suggest a higher crystallinity for these samples. Crystal morphology of the materials was studied by scanning electron microscopy (Fig. 3). The three samples synthesised in the absence of bmp cation are constituted by agglomerates of crystals that exhibit the conventional platelike morphology characteristic of ferrierite [16,17]. However, there are differences in crystal size.
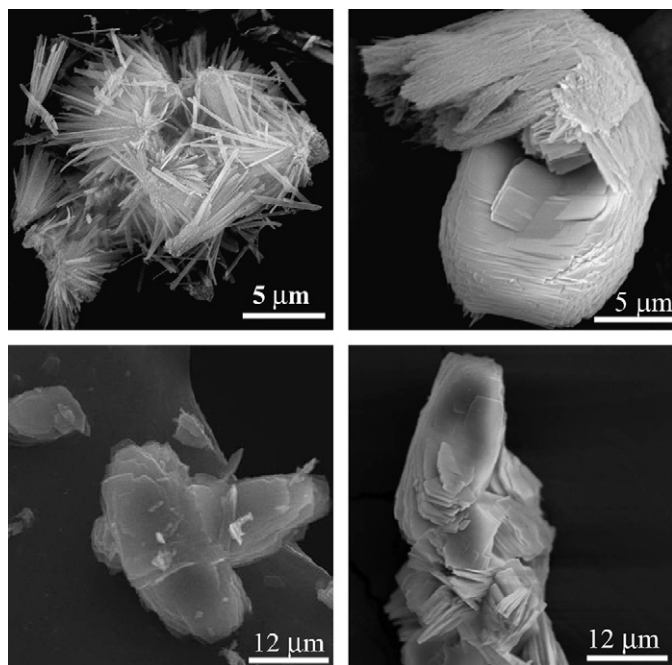
Fig. 3. SEM images of the samples FER-bmp-TMA obtained after 20 d of hydrothermal treatment (up, left), FER1 obtained after 14 d (up, right), FER-pyrr-TMA obtained at 10 d (down, left) and FER-pyrr obtained after 10 days (down, right).

Table 2
Chemical analysis and organic content of the samples.

Sample	t (d)[b]	Chemical analysis (wt%)			C/N[c]	TGA[a] organic (wt%)	SEM/EDX Si/Al
		C	H	N			
FER-bmp-TMA	10	8.85	1.84	1.68	6.1	13.5	15.1
	20	9.3	1.83	1.73	6.3	13.7	15.5
	30	8.79	1.79	1.65	6.2	12.9	16.0
	83	8.4	1.66	1.62	6.0	11.7	15.6
FER-pyrr-TMA	7	7.81	1.85	2.03	4.5	11.8	15.4
	10	7.58	1.86	1.97	4.5	11.6	15.9
FER-pyrr	7	7.63	1.75	2.03	4.4	11.5	15.2
	10	7.35	1.74	2.00	4.3	11.2	15.0
FER1	14	5.48	1.38	1.61	4.0	9.6	15.8

[a] Weight loss in the range 200–900 °C as measured by thermogravimetric analysis.
[b] Heating time (days).
[c] Molar ratio.

The sample synthesised in presence of Na^+ at high pH possesses smaller crystals, with dimensions of 3×2.5 μm, while those of samples FER-pyrr and FER-pyrr-TMA are about 22×13 μm on average. This increase in the crystal size due to the presence of fluoride anions in the synthesis gel is commonly reported for zeolite materials [18,19]. In contrast, ferrierite obtained from gels with bmp and TMA as SDAs presents needle-like crystals ca. 7 μm long. This crystal habit has been scarcely observed for ferrierite and remarkably differs from the morphology observed for the rest of samples.

The Si/Al ratio of the crystals, measured by SEM/EDX, is within the range 15–16 for the four sets of samples (Table 2), close to the one of the synthesis gels. This result corresponds to an aluminium content of ca. 2.2 atoms per unit cell of ferrierite. ICP-AES results confirmed the presence of sodium in the FER1 samples (Na/Al molar ratio of 0.13).

The organic content of the as-made samples for different crystallisation times is collected in Table 2. The C/N atomic ratio, calculated from the elemental analysis, for the samples containing either TMA and pyrrolidine (FER-pyrr-TMA) or pyrrolidine alone (FER-pyrr and FER1) as SDAs is close to 4, the theoretical value

corresponding to these molecules. These results suggest that the organic molecules resisted the hydrothermal treatment. Within the void volume of the ferrierite structure, there are two possible locations for the organic guest molecules. They can be accommodated either in the main 10-MR channel or in the ferrierite cavity. In principle, the small size of both pyrrolidine and TMA allows them to be occluded in any of these two locations. XRD powder diffraction studies have been recently carried out in an attempt to find out the location of each organic molecule within the framework, which will provide a better understanding of their role in the crystallisation process. The organic content corresponds in both FER-pyrr and FER-pyrr-TMA samples to approximately 4 molecules per unit cell. The ferrierite framework contains two cavities per unit cell, which can host only one molecule of either TMA or pyrrolidine. Therefore, these data suggest that, of the 4 organic molecules per unit cell, 2 of them are occluded in the cavity and the other two molecules in the 10-MR channel. Preliminary XRD Rietveld refinement results of both samples support this assignment [20].

For the samples crystallised from gels containing bmp and TMA, chemical analysis and ^{13}C MAS NMR spectrum (not shown) confirmed that these organic cations kept their integrity within the zeolite. Furthermore, molecular mechanics calculations revealed the templating role of both cations. The most stable configuration of the system corresponds to the location of bmp in the 10-MR channels of the ferrierite structure, being too large to be occluded inside the small cages, while TMA is occluded within the FER cages [10]. This result was confirmed by ^{13}C CP MAS NMR, as the observed chemical shift of the ^{13}C resonance corresponding to TMA ions (57.4 ppm) was in the range of the signals reported for TMA occluded in other zeolitic cavities with a size similar to that of the FER cage [21,22]. According to the chemical analysis results, the nitrogen content of the samples is approximately 0.12 mol per 100 g of sample, which is equivalent to 3 N atoms per unit cell. Both TGA and chemical analysis (Table 2) indicate that the organic content of FER-bmp-TMA samples slightly decreases with the crystallisation time. This observation might be connected with the fact that ferrierite-related layered materials obtained by different procedures are formed by the stacking of ferrierite layers [23–27]. If the layers are not fully condensed in the as-made material, additional organic molecules could eventually be located in the interlayer space, leading to an organic content slightly higher than that expected for fully connected tridimensional crystals, as could be the case of the FER-bmp-TMA samples crystallised at shorter times.

For the samples synthesised with pyrrolidine, the amount of organic material occluded in the framework significantly varies depending on the synthesis procedure. The FER1 samples, prepared in the presence of alkaline cations, show an organic content lower than that found for the FER-pyrr samples, prepared in fluoride medium with no alkaline cations. Bearing in mind that both sets of samples present a similar Al content, this result provides an indirect evidence for the incorporation of sodium cations to the inner volume of the zeolite in the FER1 samples for negative charge compensation, which was confirmed by the ICP-AES results.

For all the samples prepared in fluoride medium, the number of organic molecules occluded within the zeolite is higher than the amount of aluminium atoms incorporated to the zeolitic network. This fact evidences that a fraction of the positive charge associated to the organic molecules employed as SDAs would be most probably counter balanced by the incorporation of fluoride anions within the void volume of the zeolite during the crystallisation process.

3.2. FTIR characterisation of hydroxyl groups

FTIR spectra in the O–H stretching region of the ferrierite samples outgassed at 400 °C are disclosed in Fig. 4. All the samples
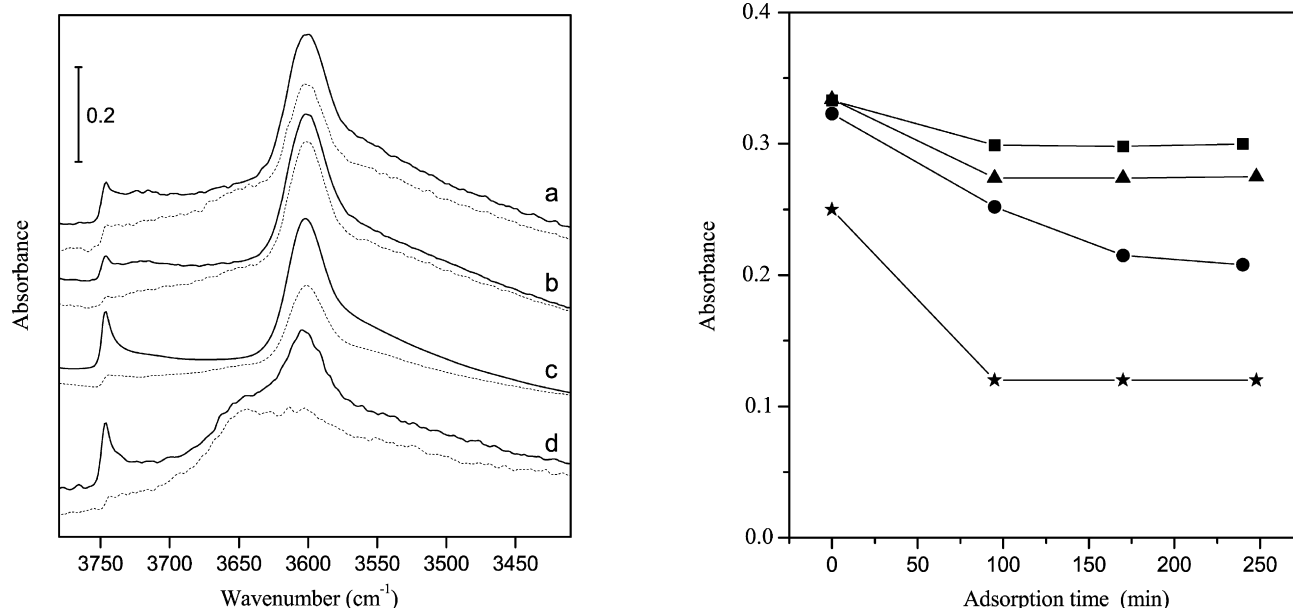
Fig. 4. Left: FTIR spectra in the ν_{OH} region of ferrierite samples after outgassing at 400 °C (full lines) and subsequent adsorption of pyridine by contact with the amine vapour at 150 °C for 4 h (dotted lines): (a) FER-pyrr-TMA obtained after hydrothermal treatment for 7 d, (b) FER-pyrr at 10 d, (c) FER-bmp-TMA at 20 d and (d) FER1. Right: Intensity of the bridging OH band at 3601 cm^{-1} as a function of pyridine adsorption time, for samples FER-pyrr-TMA (triangles), FER-pyrr (squares), FER-bmp-TMA (circles) and FER1 (stars).
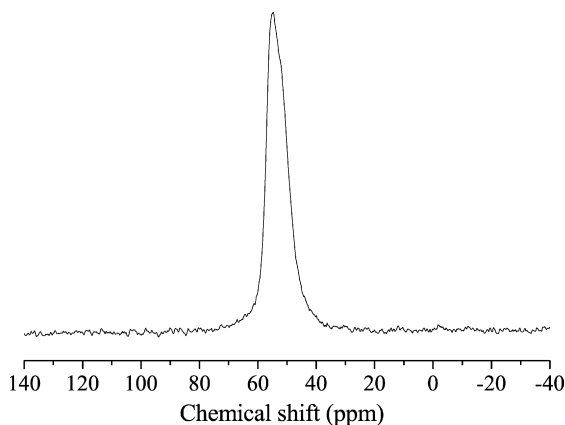

Fig. 5. ^{27}Al MAS NMR spectrum of the calcined FER-pyrr-TMA sample obtained after 10 days of heating.

exhibit an intense asymmetric band at ca. 3601 cm^{-1} with a weak shoulder at 3550 cm^{-1}, characteristic of bridging hydroxyl groups (Si–OH–Al), and a weaker band at 3747 cm^{-1}, corresponding to terminal silanols (cf. Ref. [28]). The band at 3601 cm^{-1} shows similar intensity for all the samples synthesised in fluoride medium, which indicates that all these samples possess comparable concentration of strong Brönsted sites, in agreement with their similar Si/Al ratio. The spectra do not show additional hydroxyl bands that could be attributed to extra-framework species. Indeed, in calcined sample FER-pyrr-TMA, only tetrahedrally coordinated Al species are detected by ^{27}Al MAS NMR (Fig. 5), as the spectrum shows a single resonance at around 52 ppm. The absence of a resonance corresponding to octahedral species suggests that extra-framework Al species would be present in low concentration and in a highly distorted environment. In the FTIR spectrum of sample FER1, the bridging hydroxyls band shows lower intensity, revealing that the concentration of strong Brönsted sites in this sample is around 25% lower than the amount in the samples synthesised in fluoride medium. In addition, the spectrum shows a broad shoulder at ca. 3650 cm^{-1} that has been previously observed in FTIR spectra

of ferrierite zeolite in acid form, and tentatively assigned to Al–OH species [29–31]. However, the exact nature of the hydroxyl species giving rise to the latter band has not yet been clarified. Recent results indicate that the acid strength of these hydroxyls is higher than that expected for extra-framework Al species [32].

After pyridine adsorption at 150 °C, the spectra showed characteristic bands of pyridinium ions at 1545 and 1638 cm^{-1}, and weaker bands due to pyridine interacting with Lewis sites, at 1455 and 1620 cm^{-1}. In addition, the presence of weak bands at 1445 and 1596 cm^{-1}, as well as the disappearance of the terminal silanols band at 3747 cm^{-1}, pointed out to the presence of pyridine H-bonded to silanols. A decrease in the intensity of the band located at 3601 cm^{-1} was also observed, due to the proton transfer from strong Brönsted sites to pyridine. However, this band was not completely removed when the samples remained in contact with pyridine at 150 °C for as long as 90 min. Therefore, in order to verify that pyridine adsorption reached equilibrium, FTIR spectra were recorded at increasing contact times. Fig. 4 (right) shows that the bridging hydroxyls band intensity levels off with increasing pyridine adsorption time, demonstrating that after pyridine adsorption for 90 min, equilibrium was reached for all samples except FER-bmp-TMA. For the later sample, adsorption for as long as ca. 4 h was required to reach equilibrium. The results evidence that not all the acid sites are accessible to pyridine at 150 °C. It is noteworthy that the samples exhibit apparent differences on accessibility of the bridging hydroxyls to pyridine. Besides, the intensity of the band at 3650 cm^{-1} observed in the spectra of sample FER1 remained constant, indicating that these hydroxyl species were not accessible to pyridine. Nevertheless, complete removal of this band was observed when less bulky basic probe molecules, such as ammonia and CO, were adsorbed [32].

The location and accessibility of Si(OH)Al groups in ferrierite has been extensively studied, as this is a key factor which determines the catalytic properties of this zeolite. Martucci et al. [33], in a neutron powder diffraction study of deuterated ferrierite carried out at 2 K, identified two Brönsted acid sites, one of them heading towards the centre of the ferrierite cage, and the second one heading towards the 10-membered ring channel. The first one corresponds to a hydroxyl group bridging Si and Al atoms both

Table 3
Accessibility of the Brönsted acid sites to pyridine found in the IR adsorption experiments for the samples synthesised with the different combinations of SDAs.

Sample	% of acid sites accessible to pyridine
FER-pyrr	10
FER-pyrr-TMA	18
FER-bmp-TMA	36
FER1	52

located in T4 positions, and the second one bridging T1 and T3 cations (Fig. 1). Nonetheless, it is important to note that due to the low temperature at which this study was conducted, only the most stable location for the acidic hydroxyl can be found. In contrast, in an FTIR study of ferrierite samples conducted at room temperature, Zholobenko et al. [34] proposed up to four framework hydroxyls in pores of different size. These hydroxyls were assigned to Si(OH)Al groups in the 10-MR channel, in the extended ring at the intersection of 8- and 6-MR channels, and in 8- and 6-membered rings. Wichterlová et al. [28] reported on the inability for pyridine to probe all the Brönsted sites in ferrierite when adsorbed at relatively low temperatures (130 °C). This was attributed to the constrained access of pyridine to Brönsted sites located inside the ferrierite cavity. Nevertheless, it has been proposed that pyridine can pass the 8-MR window and that a combination of high temperature and pyridine partial pressure allows to quantitatively probe Brönsted acidity in ferrierite [35].

In our experimental conditions, the ferrierite samples exhibited marked differences on accessibility of pyridine to acidic hydroxyls (Table 3). In sample FER1, 52% of the bridging hydroxyls were accessible to pyridine. This value is in good agreement with previous pyridine adsorption measurements carried out on a commercial ferrierite (Si/Al ratio of 8.4), for which 60% of the Brönsted sites were found accessible to pyridine at 130 °C [28]. In comparison with the reference sample, the zeolites synthesised in fluoride medium exhibited lower accessibility, being this value strongly dependent on the combination of SDAs used. Among the later samples, the one synthesised with bmp and TMA cations (FER-bmp-TMA) showed the highest accessibility (36%). The number of Brönsted sites accessible to pyridine decreased to 18% when bmp cations were replaced by pyrrolidine in the synthesis gel (sample FER-pyrr-TMA), and it decreased further to 10% when also TMA cations were replaced by pyrrolidine (sample FER-pyrr). These results evidence that the distribution of strong Brönsted acid sites between the ferrierite cages and the more accessible sites exposed to the 10-MR channels is determined by the actual combination of SDAs used in the synthesis of ferrierite. It is worth noting that the accessibility of a given Brönsted acid site is not only determined by which one is the T site that is occupied by the Al atom, but also by which one of the four oxygen atoms in its first coordination shell the proton is bound to. Hydroxyl groups associated to Al atoms in T4 sites would be non accessible to pyridine, as the four possible locations for a hydroxyl next to a T4 site are inside the ferrierite cage (Fig. 1). Furthermore, the zeolites might also contain non accessible Brönsted sites associated to Al atoms located in T1, T2 and T3 sites, even though they are in the 10-membered rings, for only 3 of the 4 oxygen atoms surrounding each one of these sites are also located in the 10-ring channel while the fourth oxygen atom is inside the ferrierite cavity. Therefore, the presence of strong Brönsted sites non accessible to pyridine could eventually be related not only to Al atoms located in T4 sites but also to some specific locations of the bridging OH species in the framework next to a given Al atom.

The organic content determined for the as-synthesised samples indicates that every ferrierite cage is occupied by one SDA cation. It is therefore expected that, at most, one T4 site per cavity (i.e. two T4 sites per unit cell) can be occupied by Al. On the other

hand, the Al content of these samples corresponds to ca. 2.2 Al atoms per unit cell. Therefore, up to 91% of the Al could be located in T4 sites and, hence, have an associated bridging hydroxyl inside the ferrierite cage. In this case, pyridine would be accessible to at most 9% of the total acid sites, a situation that would correspond to the sample synthesised in fluoride medium from pyrrolidine as the only SDA (FER-pyrr), for which 10% of acid sites interact with pyridine. This is the sample with the less accessible acid sites. Replacement of pyrrolidine by other SDA molecules led to the systematic changes in acid sites accessibility described above, which can be rationalised as follows. It has been observed that partial replacement of pyrrolidine by TMA increases accessibility (sample FER-pyrr-TMA compared to sample FER-pyrr). Preliminary XRD refinement results of sample FER-pyrr-TMA together with molecular dynamics calculations [20] show the preferential location of TMA in the ferrierite cage. Some of the cages would be filled with this cation, while others still contain pyrrolidine, with no TMA present in the main channel. Hence, the partial replacement of pyrrolidine by TMA seems to "pump" protons from inaccessible cage locations to those in more open environment accessible from the main channel.

When all the pyrrolidine molecules in the cages are replaced by TMA and those in 10-MR channels by bmp (sample FER-bmp-TMA compared to sample FER-pyrr-TMA), the average accessibility of acid sites further increases. In this way, more Al atoms are driven to positions where the associated bridging OH groups are more readily available to interact with pyridine.

An additional increase in accessibility is obtained for samples synthesised in the presence of both Na$^+$ cations and pyrrolidine. The inorganic cations could be located either in the channel or in the cage, and therefore it would not be straightforward to account for the observed effect in terms of cation location. It is worth to note that it has been shown that Na$^+$ ions are preferentially located in the ferrierite cage after partial ion-exchange of NH$_4^+$-ferrierite [36]. However, inclusion of Na$^+$ ions together with pyrrolidine species into the pores during the zeolite synthesis could lead to a different preferential location of Na$^+$ ions.

In order to rationalise all these results, it would be possible to establish a relative trend for Al location on either cage or channel sites among the several templates, as follows. For cage sites, pyrrolidine would have higher tendency than TMA to attract Al, while for channel locations the order would be pyrrolidine > bmp. In this way, the fraction of Al located at accessible 10-MR channel sites could eventually be tailored as a function of the particular selected combination of SDAs, for each one seems to possess some specific influence toward Al sitting in its vicinity.

3.3. Activity of the ferrierite samples in m-xylene isomerisation and 1-butene skeletal isomerisation

The observed differences in acid sites accessibility should have consequences on the catalytic activity of these ferrierite materials in acid-catalysed reactions. To check this influence, the catalytic transformation of two molecules with different size have been studied, the isomerisation/disproportionation of the relatively bulky *m*-xylene, and the skeletal isomerisation of the comparatively smaller 1-butene. The results are collected in Table 4. In both cases, large differences in the overall reaction rates are observed among the different samples, being the most active the one synthesised at high pH in the presence of Na$^+$ with pyrrolidine as SDA (FER1 sample). Interestingly, among the catalysts prepared in presence of fluoride anions, the one obtained from gels containing pyrrolidine as the only SDA presents the lowest activity.

In the case of *m*-xylene reaction, the synthesis method employed to obtain the ferrierite catalysts has also a significant influence on the *p*-xylene/*o*-xylene ratio. The most active catalyst

Table 4
Activity and selectivity of the different samples in the isomerisation–disproportionation of *m*-xylene and in the 1-butene isomerisation.

Sample	*m*-Xylene isomerisation			*n*-Butene isomerisation		
	Reaction rate[b] (mol/(g h))	P/O ratio	I/D ratio	X^c (%)	$S_{(i-C_4^=)}$ [d] (%)	S_{BET} (m^2/g)
FER-pyrr[a]	5.60E−04	n.d.	n.d.	9.6	79.3	350
FER-pyrr-TMA	6.40E−03	1.4	4.3	14.8	79.1	341
FER-bmp-TMA	2.20E−02	1.4	10.9	24.0	69.2	305
FER1	3.90E−02	4.6	46.2	40.2	24.6	244

[a] Conversion lower than 0.1%.
[b] Calculated for conversions lower than 5%.
[c] Conversion at time-on-stream = 30 min.
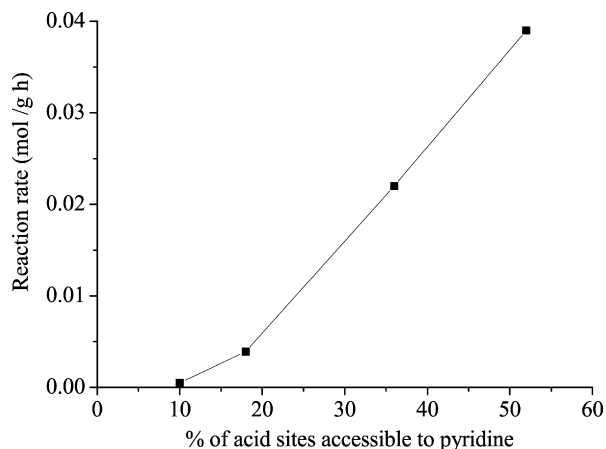[d] Selectivity to isobutene (time-on-stream = 30 min).

Fig. 6. Activity of the different samples in *m*-xylene isomerisation as a function of the accessibility of pyridine to their acid sites in the IR experiments.

(FER1) exhibits the expected *p/o* ratio for zeolites with one-directional 10-MR channels [37–39], and a negligible disproportionation activity, which indicates that the reaction occurs mainly within the 10-MR channels, with a very small contribution of the external surface. On the contrary, the samples synthesised in fluoride medium show relatively low *p/o* values, and comparatively higher disproportionation activity than the one obtained at high pH. This higher tendency to yield *o*-xylene and disproportionation products is an indication of a more open environment and less diffusional restrictions for the reaction in the catalysts synthesised in fluoride medium. This implies that in the latter catalysts the ratio between the number of accessible acid sites on the external surface and the number of accessible acid sites in the bulk would be higher than that of sample FER1. Despite this fact, the samples prepared in fluoride medium present lower activity than FER1, which suggests that a larger fraction of active centres would not be accessible to the *m*-xylene molecule. Indeed, these differences in activity could not be accounted for by differences in surface area. Table 4 shows an opposite trend between surface area and activity, i.e., the sample with the lowest activity possesses the highest surface area. This result, consistent with the obtained *p/o* values, is an additional evidence that the relative contribution of sites located in external surface to the overall activity of the samples prepared in fluoride medium would be higher than that of the one obtained in alkaline medium, and suggests that the reaction is barely affected by the reported differences in crystal size among the different catalysts. Hence, the observed differences in activity should be attributed to differences in the accessibility of the reactant *m*-xylene molecules to the acid sites of the ferrierite samples we have prepared. Fig. 6 depicts the relationship between the activity of the catalysts and the acid sites accessibility. Strong Brönsted sites accessibility is given as percentage of the total number of bridging
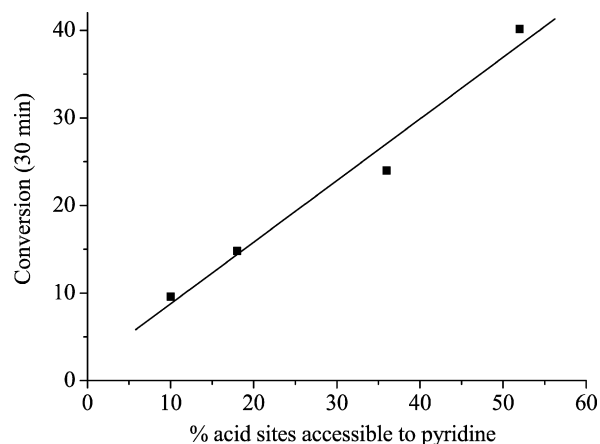

Fig. 7. Activity of the different samples in 1-butene isomerisation (time-on-stream = 30 min) as a function of the accessibility of pyridine to their acid sites in the IR experiments.

hydroxyls that protonate pyridine after prolonged adsorption. For the samples synthesised in fluoride medium, this parameter would be proportional to the number of acid sites per unit mass of catalyst that can be reached by pyridine and protonate this molecule, as all these zeolites possess similar density of bridging hydroxyls. For sample FER1, however, it has to be taken into account that the concentration of bridging hydroxyls is ca. 25% lower. Nevertheless, due to the significantly higher acid sites accessibility determined for that sample, it would possess the largest content of acid sites able to protonate pyridine. It can be clearly observed in Fig. 6 that the activity in the *m*-xylene isomerisation increases with the fraction of acid sites that interact with pyridine. However, it is interesting to note that the relationship between catalytic activity and number of acid sites accessible to pyridine is not linear. The increase of activity is more prominent as the number of accessible OH groups increases. This result suggests that a fraction of the hydroxyl groups that are able to interact with pyridine at 150 °C are not available to activate the bulkier *m*-xylene even at such high temperature as 350 °C, the temperature at which the catalytic test has been performed.

In contrast to results on *m*-xylene conversion, when the isomerisation of the smaller 1-butene molecule is considered, a nearly linear relationship between acidity and activity is found for the samples synthesised in fluoride medium (Fig. 7) in agreement with its molecular size being smaller than that of *m*-xylene. These observations suggest that hydroxyl groups other than those buried inside the cage and associated to T4 sites might be available for reaction if appropriate substrate molecules are used. These Brönsted sites would be associated to the Al atoms located in T1, T2 and T3 positions, which would not be equivalent in terms of their accessibility from the 10-MR channel for bulky molecules. It has been reported [40–42] that the formation of isobutene on ferrierite catalysts is a function of the number of acid hydroxyl groups located in the 10-MR channel, which is consistent with the acidity results reported here. A complete account of the catalytic behaviour of these samples in 1-butene conversion is reported elsewhere [43]. It is worth to note that the catalyst FER1 do not seem to follow the linear relationship between activity and density of accessible bridging hydroxyls found for the samples synthesised in fluoride medium, taking into account that the estimated density of bridging hydroxyls in catalyst FER1 is ca. 25% lower. This result might be explained assuming that at least part of the hydroxyl species responsible for the band at 3650 cm^{-1}, which are not accessible to pyridine, could be accessible and able to activate 1-butene.

The analysis of the characterisation and catalytic activity results discussed above strongly supports the conclusion that the accessi-

bility of acid sites to the relatively bulky reagent molecules like pyridine, *m*-xylene and butene in these samples is strongly dependent on the specific combination of structure directing agents used in the synthesis. It is interesting to observe that the presence of sodium ions in the gel is sufficient to enormously increase the acid site accessibility, as can be seen by comparing the results corresponding to the sample synthesised in fluoride medium using pyrrolidine as SDA (FER-pyrr) with that obtained at high pH in the presence of the same SDA (FER1). On the other hand, significant differences in the accessibility of the acid sites among the catalysts prepared in fluoride medium have been evidenced. In this case the negative charge associated to the aluminium atoms can only be neutralised by the bulky organic SDAs, as there are no sodium cations present in the synthesis gel. Therefore, these differences in the accessibility of the acid centres are an indication that the specific organic SDA employed in each case have a marked effect on the location pattern of Al atoms associated to these acid sites in the framework. In other words, we have found evidences that strongly suggest that the Al location in the ferrierite framework can be influenced in a decisive manner by the structure directing agents present in the gel, including sodium among them.

Regarding the effect of the different SDA, the results we present suggest that this effect would be dependent upon the particular template molecules used in the synthesis, although we can not yet offer a clear explanation as to why specific combination of template molecules behave so differently. As compared with the small sodium cation, which would be able to occupy a variety of different positions, the bulkiness of the organic SDAs would fix them in some specific configuration inside of either the main channel or the cage, making the Al sitting much more specific as well.

4. Conclusions

Ferrierite crystals having the same Al content, 2.2 Al/u.c., have been synthesised from sodium-free gels in fluoride media by using some specific combinations of structure directing agents, namely tetramethylammonium (TMA), pyrrolidine and benzylmethylpyrrolidinium (bmp). It has been found that the distribution of bridging hydroxyl groups between the ferrierite cage accessible through 8-MR windows and the 10-MR channel varies according to the specific combination of templates used in the synthesis. Considering also the reference ferrierite sample synthesised in alkaline medium from a gel containing both Na$^+$ and pyrrolidine, the accessibility of pyridine to the Brönsted acid sites at 150 °C decreases in the order Na/pyrrolidine > TMA/bmp > TMA/pyrrolidine > pyrrolidine. A good correlation between acid sites accessibility and catalytic activity in the isomerisation of *m*-xylene and conversion of *n*-butene has been found. Hence, this synthesis strategy of ferrierite crystals allows to gain an effective control on acid sites distribution in the zeolite framework, and might eventually be extended to other suitable zeolite materials by a rational choice of appropriate structure directing agents.

Acknowledgments

Supplementary material

The online version of this article contains additional supplementary material.

Please visit DOI: 10.1016/j.jcat.2009.02.017.

References

[1] B. Wichterlová, J. Dědeček, Z. Sobalík, J. Čejka, Stud. Surf. Sci. Catal. 135 (2001) 344.
[2] J. Dědeček, D. Kaucký, B. Wichterlová, O. Gonsiorová, Phys. Chem. Chem. Phys. 4 (2002) 5406.
[3] V. Gábová, J. Dědeček, J. Čejka, Chem. Commun. (2003) 1196.
[4] J. Dědeček, J. Čejka, M. Oberlinger, S. Ernst, Stud. Surf. Sci. Catal. 142 (2002) 23.
[5] http://iza-structure.org/databases.
[6] P.A. Vaughan, Acta Crystallogr. 21 (1966) 983.
[7] R.E. Morris, S.J. Weigel, N.J. Henson, L.M. Bull, M.T. Janicke, B.F. Chmelka, A.K. Cheetham, J. Am. Chem. Soc. 116 (1994) 11849.
[8] M.P. Attfield, S.J. Weigel, F. Taulelle, A.K. Cheetham, J. Mater. Chem. 10 (2000) 2109.
[9] Y. Yokomori, J. Wachsmuth, K. Nishi, Microporous Mater. 50 (2001) 137.
[10] A.B. Pinar, L. Gómez-Hortigüela, J. Pérez-Pariente, Chem. Mater. 19 (2007) 5617.
[11] A.B. Pinar, R. García, J. Pérez-Pariente, Collect. Czech. Chem. Commun. 72 (2007) 666.
[12] A.B. Pinar, J. Pérez-Pariente, L. Gómez-Hortigüela, WO2008116958-A1.
[13] D.F. Shantz, R.F. Lobo, C. Fild, H. Koller, Stud. Surf. Sci. Catal. 130 (2000) 845.
[14] K. Frolich, R. Bulánek, P. Nachtigall, in: Proc. of the 40th Symp. on Catalysis, Prague, 2008, p. 40.
[15] C.J. Plank, E.J. Rosinski, M.K. Rubin, US Patent 4 016 245 (1977).
[16] A. Kuperman, S. Nadimi, S. Oliver, G.A. Ozin, J.M. Garces, M.M. Olken, Nature 365 (1993) 239.
[17] W.J. Smith, J. Dewing, J. Dwyer, J. Chem. Soc. Faraday Trans. 1 85 (1989) 3623.
[18] J.L. Guth, H. Kessler, R. Wey, Stud. Surf. Catal. Sci. 28 (1986) 121.
[19] L.A. Villaescusa, M.A. Camblor, Recent Res. Devel. Chem. 1 (2003) 93.
[20] A.B. Pinar, et al., manuscript in preparation.
[21] W. Fan, S. Shirato, F. Gao, M. Ogura, T. Okubo, Microporous Mesoporous Mater. 89 (2006) 227.
[22] S. Hayashi, K. Suzuki, K. Hayamizu, J. Chem. Soc. Faraday Trans. 1 85 (1989) 2973.
[23] L. Schreyeck, P. Caullet, J.C. Mougenel, J.L. Guth, B. Marler, Microporous Mater. 6 (1996) 259.
[24] T. Ikeda, Y. Akiyama, Y. Oumi, A. Kawai, F. Mizukami, Angew. Chem. Int. Ed. 43 (2004) 4892.
[25] A. Burton, R.J. Accardi, R.F. Lobo, Chem. Mater. 12 (2000) 2936.
[26] D.L. Dorset, G.J. Kennedy, J. Phys. Chem. B 108 (2004) 15216.
[27] R. Millini, L.C. Carluccio, A. Carati, G. Bellussi, C. Perego, G. Cruciani, S. Zanardi, Microporous Mesoporous Mater. 74 (2004) 59.
[28] B. Wichterlová, Z. Tvarůžková, Z. Sobalík, P. Sarv, Microporous Mesoporous Mater. 24 (1998) 223.
[29] Y.S. Jin, A. Auroux, J.C. Vedrine, Appl. Catal. 37 (1988) 1.
[30] M. Trombetta, G. Busca, S. Rossini, V. Piccoli, U. Cornaro, A. Guercio, R. Catani, R.J. Willey, J. Catal. 179 (1998) 581.
[31] V.L. Zholobenko, E.R. House, Catal. Lett. 89 (2003) 35.
[32] B. Onida, et al., manuscript in preparation.
[33] A. Martucci, A. Alberti, G. Cruciani, P. Radaelli, P. Ciambelli, M. Rapacciuolo, Microporous Mesoporous Mater. 30 (1999) 95.
[34] V.L. Zholobenko, D.B. Lukyanov, J. Dwyer, W.J. Smith, J. Phys. Chem. B 102 (1998) 2715.
[35] J.A.Z. Pieterse, S. Veefkind-Reyes, K. Seshan, L. Domokos, J.A. Lercher, J. Catal. 187 (1999) 518.
[36] P. Sarv, B. Wichterlová, J. Čejka, J. Phys. Chem. B 102 (1998) 1372.
[37] J. Martens, J. Pérez-Pariente, E. Sastre, A. Corma, P.A. Jacobs, Appl. Catal. 45 (1988) 85.
[38] A. Corma, E. Sastre, J. Catal. 129 (1991) 177.
[39] G. Mirth, J. Čejka, J.A. Lercher, J. Catal. 139 (1993) 24.
[40] B. Wichterlová, N. Žilkova, E. Uvanova, J. Čejka, P. Sarv, C. Paganini, J.A. Lercher, Appl. Catal. A 182 (1999) 297.
[41] L. Domokos, L. Lefferts, K. Seshan, J.A. Lercher, J. Mol. Catal. A Chem. 162 (2000) 147.
[42] J. Čejka, B. Wichterlová, P. Sarv, Appl. Catal. A 179 (1999) 217.
[43] C. Márquez-Alvarez, A.B. Pinar, R. García, M. Grande-Casas, J. Pérez-Pariente, Top. Catal., in press.